[3]N. Bloembergen and T. J. Rowland, Phys. Rev. 97, 1679 (1955).
[4]R. J. Snodgrass and L. H. Bennett, Phys. Rev. 132, 1465 (1963).
[5]H. Alloul and C. Froidevaux, Phys. Rev. 163, 324 (1967).
[6]H. Alloul and R. Deltour, Phys. Rev. 183, 414 (1969).
[7]P. W. Anderson and P. R. Weiss, Rev. Mod. Phys. 25, 269 (1953).
[8]P. W. Anderson, J. Phys. Soc. Japan 9, 316 (1954).
[9]S. N. Sharma, D. Ll. Williams, and H. E. Schone, Phys. Rev. 188, 662 (1969).
[10]L. Tterlikkis, S. D. Mahanti, and T. P. Das, Phys. Rev. Letters 21, 1796 (1968).
[11]C. H. Townes and W. D. Knight, Phys. Rev. 77, 852 (1950).
[12]A. Abragam, *Principles of Nuclear Magnetism* (Oxford U.P., London, 1961).
[13]M. H. Boon, Physica 30, 1326 (1964).
[14]A. C. Chapman, P. Rhodes, and E. F. W. Seymour, Proc. Phys. Soc. (London) 70B, 345 (1957).
[15]H. Wahlquist, J. Chem. Phys. 35, 1708 (1961).
[16]D. E. O'Reilly and T. Tsang, Phys. Rev. 128, 2639 (1962).
[17]E. R. Andrew, Phys. Rev. 91, 425 (1953).
[18]S. D. Mahanti and T. P. Das, Phys. Rev. 170, 426 (1968); L. Tterlikkis, S. D. Mahanti, and T. P. Das, *ibid.* 178, 630 (1969).
[19]J. R. Anderson and A. V. Gold, Phys. Rev. 139, 1459 (1965).
[20]H. Alloul and C. Froidevaux, Colloq. Ampere 14, 457 (1966).
[21]C. Kittel and A. Abrahams, Phys. Rev. 90, 238 (1953).
[22]V. Heine, *Group Theory in Quantum Mechanics* (Pergamon, London, 1960).
[23]E. B. Baker, J. Chem. Phys. 26, 960 (1957).

PHYSICAL REVIEW B VOLUME 5, NUMBER 11 1 JUNE 1972

Effect of Primary-Electron Diffusion on Secondary-Electron Emission

Alan J. Bennett and Laura M. Roth
General Electric Research and Development Center, Schenectady, New York 12301
(Received 3 November 1971)

We consider some effects of primary-electron diffusion on secondary-electron emission from a free-electron model of a polycrystalline target—in particular the angular distribution and energy dependence of the secondaries. The distributions of primary electrons due to incident 2- and 10-keV monoenergetic beams are obtained by means of a Boltzmann equation. The fraction of back-scattered primaries is found to be in good agreement with experiment. The primary distributions excite distributions of secondary electrons which diffuse toward and are transmitted through the surface. In accord with experiment the large angular ansiotropy in the emitted secondary-electron distribution predicted by Stoltz is found to be greatly reduced by the primary diffusion. The transmission coefficient, not included in previous calculations, is also of importance in determining the characteristics of the observed secondaries.

I. INTRODUCTION

The problem of secondary-electron emission[1-3] has received renewed interest recently in part due to the development of the scanning electron microscope. An extensive review of the previous work on this complete subject has been given by Hachenberg and Brauer.[1] Briefly, when a target is bombarded with primary electrons of a given energy and direction relative to the surface normal, secondary electrons (< 50 eV) are emitted with a current distribution $j_s^0(E, \Omega)$, which is a function of secondary energy E and direction Ω. Due to the difficulty of the measurements, most experiments yield information about various integrals of $j_s^0(E, \Omega)$. These are the pure angular distribution $j_s^0(\Omega) = \int j_s^0(E, \Omega) dE$, the pure energy distribution $j_s^0(E) = \int j_s(E, \Omega) d\Omega$, and the yield $= \int\int j_s^0(E, \Omega) dE\, d\Omega$.

Jonker[4] measured $j_s^0(E, \Omega)$ for primaries normally incident on polycrystalline Ni and found that the angular distribution of the secondary current obeyed a cosine law characteristic of an isotropic distribution of secondaries inside the material. On the other hand, theoretical calculations primarily due to Stoltz[5] predicted an angular distribution which is considerably flattened.

We consider in this paper the effect of primary-electron diffusion on secondary-electron emission, in particular, on the angular distribution and energy dependence of secondaries when the primary energy is 2 and 10 keV. The latter primary energy is characteristic of scanning-electron-microscope operation. One aim of this work is to resolve the above-mentioned discrepancy regarding the angular dependence. Another aim is to calculate the pure energy distribution as a function of primary direction and energy. Experimentally, the yield is found to increase with increasing primary energy up to about 500 eV and then to decrease. For a fixed primary energy the yield increases as the primary beam deviates from normal incidence. This is often attributed to the

increased number of secondaries created near the surface.[3]

We confine our attention in the present work to polycrystalline targets. Single-crystal targets exhibit angular distributions[6] and yields[7] of secondaries characterized by sharp structure which is quite sensitive to the direction of incident primaries. These interesting features are related to the crystalline structure[8] which we are ignoring in this first calculation.

We can view the events leading to secondary-electron emission in three stages: (a) The primary electrons enter the sample, scatter, and lose energy; (b) these primary electrons excite secondary electrons; (c) the secondary electrons move toward the surface and pass through the potential barrier.

The distribution of high-energy electrons upon traversing a material has been of interest for a long time. In the early work of Bethe, Rose, and Smith,[9] it was noted that there are two basic processes—elastic scattering by the nuclei which primarily changes the incoming electron's direction and inelastic scattering by the electrons of the material (including secondary emission!) which accounts primarily for the energy loss. This work introduced a Boltzmann-equation treatment of the problem and further assumed that multiple small-angle scattering was more important than large-angle Rutherford scattering. In further work with MeV electrons in thin foils and infinite media, Snyder and Scott,[10] Lewis,[11] and Spencer,[12] showed that scattering through both small and large angles can be of importance for high-energy primaries in low-Z materials. Lewis[11] showed that all scattering angles could be treated using an integral form of the diffusion term in the Boltzmann equation.

In considering the semi-infinite medium, Archard[13] investigated electron backscattering using a rather crude model and concluded that the multiple small-angle scattering accounted for backscatter for sufficiently high Z for 100-kV electrons, while single large-angle scatterings[14] were important for lower Z. Dashen,[15] however, argued that both mechanisms should be of some importance for all Z. The semi-infinite medium has been treated in connection with x-ray production by Green[16] using a Monte Carlo treatment which includes all angle scattering, and by Brown,[17] who used a numerical treatment of the Bethe-Rose-Smith (BRS)[9] diffusion equation.

In Sec. II we use a modification of Brown's[17] method for obtaining a primary-electron distribution to use in obtaining the secondary-source function. Based as it is on the BRS diffusion equation, this calculation includes the small-angle scattering and not the large-angle scattering. This appears to be adequate for the range of energy and Z considered but we remark that a similar treatment could be applied to Lewis's equation.

Considering now the second stage of the process, the rate of production of secondary electrons, i.e., the secondary-electron source function, is generally calculated in second-order quantum perturbation theory[1,5,18] with the use of a (screened) Coulomb interaction. In the case of a fixed primary-electron density and velocity, within the free-electron model (intraband case), electrons are preferentially created with velocities perpendicular to the primary beam. This is the source of the pronounced anisotropy in Stoltz's[5] calculation which was not observed in Jonker's experiments. The interband case has not been considered in detail but shows somewhat less anisotropy.[1]

In Sec. III our distribution of primary electrons is used to obtain the source function for secondary electrons, using free-electron theory with an unscreened Coulomb interaction.

The third stage is generally broken into two—the electron transport and transmission through the surface barrier. The secondary-electron transport has been considered by Wolff[19] using the Boltzmann equation and techniques introduced by Weymouth.[20] Wolff treated only an essentially spatially homogeneous isotropic source. Stoltz,[5] ignoring the presence of the surface, has considered a spatially homogeneous but anisotropic source. The source anisotropy was reduced but not eliminated by the interaction between the emitted electrons.

The refraction of the secondary electrons by the surface barrier has been treated previously but no barrier transmission factor seems to have been included in previous work.[5] We have considered transport and transmission together because, in fact, the boundary conditions at the surface are an important part of the transport problem and should ideally be considered together with the spatial inhomogeneity of the source function.

In Sec. IV we introduce our source function into the Boltzmann-equation approach due to Wolff[19] to describe the transport of secondary electrons to the surface. The complete boundary-value problem with a spatially varying source function has not been solved. We have developed methods of dealing approximately with either a spatial variation of the source function or the presence of the boundary, and these are presented and compared.

The results of the specific calculation for 2- and 10-keV electrons incident on a free-electron-like material with $Z = 28$, $A = 60$, i.e., characteristic of Ni and $E_F = 4.6$ eV are presented in Sec. V. (We originally intended to use all the parameters characteristic of Ni, but its free electron E_F is, in fact, somewhat larger than that inadvertently used

here.) Energy, angular, and spatial distributions of primary and secondary electrons are given and compared with previous theoretical and experimental results.

II. DISTRIBUTION OF PRIMARY ELECTRONS

We first describe the Boltzmann-equation approach due to Bethe, Rose, and Smith[9] which we use to obtain the primary-electron distribution $f(\vec{K}, \vec{r}_p)$, where f is the number of electrons in the volume $d^3K d^3r_p$ of phase space. Brown[17] has used this method to calculate x-ray excitation effects. Assuming small-angle scattering, a unique relationship between the electron's energy $\mathcal{E}$ and the path length s it traverses in the material, and a stationary situation, Bethe *et al.* obtained

$$\frac{\partial f(s, \vec{u}, \vec{r}_p)}{\partial s} = -\vec{u}\cdot\nabla_{\vec{r}_p} f(s, \vec{u}, \vec{r}_p) + \frac{1}{\lambda(s)} \nabla^2_{\vec{u}} f(s, \vec{u}, \vec{r}_p) . \quad (2.1)$$

Here $\vec{u}$ is a unit vector in the direction of the electron velocity and

$$\nabla^2_{\vec{u}} = \frac{1}{\sin\theta_1}\frac{\partial}{\partial\theta_1}\left(\sin\theta_1 \frac{\partial}{\partial\theta_1}\right) + \frac{1}{\sin^2\theta_1}\frac{\partial^2}{\partial\varphi_1^2} , \quad (2.2)$$

where θ_1 is the angle between $\vec{u}$ and the inward normal to the surface and φ_1 is the azimuthal angle. The transport mean free path is given by

$$\frac{1}{\lambda(s)} = \pi N \int (\sin\alpha)\sigma(\alpha, s)(1-\cos\alpha)d\alpha , \quad (2.3)$$

where $\sigma(\alpha, s)$ is the cross section for deflection by an angle α of an electron which has traveled a distance s, due to an atom of the metal, and N is the number of those atoms per unit volume. Bethe *et al.*[9] determined an approximate expression for the mean free path which we use here:

$$\frac{1}{\lambda(\mathcal{E})} = 1.986\times10^4 \frac{Z^2}{A\mathcal{E}^2} \ln\left(\frac{17.3\,\mathcal{E}^{1/2}}{Z^{1/3}}\right) , \quad (2.4)$$

where Z is the nuclear charge of the scattering atom, A is its atomic number, and $\mathcal{E}$ and λ are expressed in keV and cm, respectively.

Various expressions, both semiempirical and more rigorous, have been obtained for the energy of an electron as a function of the distance s it travels in a material. We use here an empirical function used by Brown and Ogilvie[17,21]

$$s = \frac{0.33\times10^{-5}A}{\rho Z}(\mathcal{E}_{\max}^{1.7} - \mathcal{E}^{1.7}) , \quad (2.5)$$

where ρ is the density of the scattering material (g/cm^3), $\mathcal{E}_{\max}$(keV) is the initial electron energy, and s is the range (cm). This has the functional dependence of the semiempirical Webster law but the constant prefactor is adjusted to give agreement with the total range predicted by a more complicated expression due originally to Bethe.[22] The energy and mean free path are plotted versus the range in Fig. 1.

For a normally incident monoenergetic beam, constant over the surface, Eq. (2.1) reduces to

$$\frac{\partial}{\partial s} f(s, \theta_1, x) = -\cos\theta_1 \frac{\partial}{\partial x} f(s, \theta_1, x) + \frac{1}{\lambda(s)\sin\theta_1}\frac{\partial}{\partial\theta_1}\sin\theta_1 \frac{\partial f}{\partial\theta_1}(s, \theta_1, x), \quad (2.6)$$

where x is measured in from the surface as shown in Fig. 2. This differential equation was converted to a difference equation and solved numerically by Brown.[17] We found, however, that the detailed method adopted by Brown presents various difficulties as described below. It was therefore necessary to reformulate the calculation. We first change the angular variable to $u = \cos\theta_1$, so that Eq. (2.6) becomes

$$\frac{\partial}{\partial s} f(s, u, x) = -u\frac{\partial}{\partial x} f(s, u, x) + \frac{1}{\lambda(s)}\frac{d}{du}(1-u^2)\frac{d}{du} f(s, u, x) . \quad (2.7)$$

The boundary conditions are that at zero path ($s = 0$) we have an incoming collimated beam:

$$f(0, u, x) = \text{const}\times\delta(u-1)\delta(x) , \quad (2.8)$$

while for lower energies the particles are outgoing at the boundary:

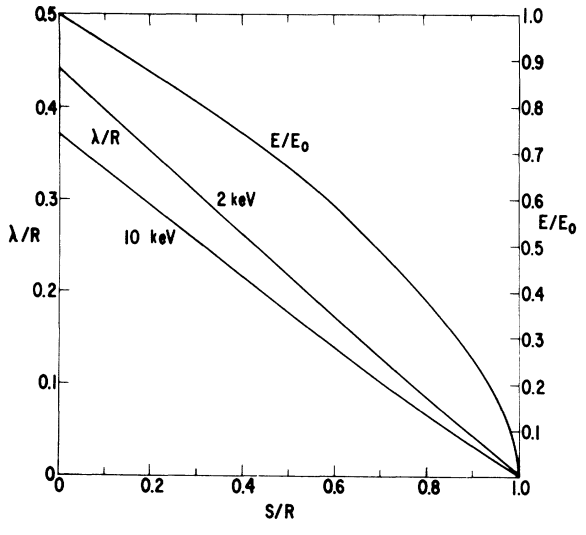

FIG. 1. Mean free path [Eq. (2.4)] and energy [Eq. (2.5)] of 2- and 10-keV primary electrons as a function of the path length traversed s. Lengths are given in units of the total range R and energies in units of the initial energy E_0.

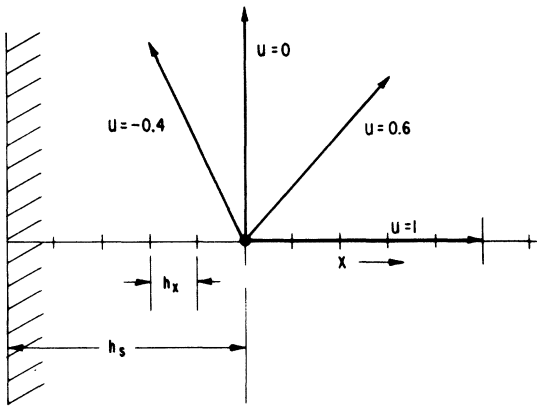

FIG. 2. Intervals of path length h_s and distance perpendicular to the surface h_x.

$$f(s, u, 0) = 0, \quad s > 0, \quad u > 0. \tag{2.9}$$

We also require f to vanish for $s \geq R$ and $x \geq R$, where R is the range. We now convert Eq. (2.7) to a difference equation. We divide x, s, and u into intervals of width h_x, h_s, and h_u, respectively. We assume, in particular, that $h_u = 1/N_u$, where N_u is an integer. We then let

$$\begin{aligned} s &= l h_s , \\ x &= m h_x , \\ u &= 1 - n h_u . \end{aligned} \tag{2.10}$$

There is some arbitrariness in converting the differential equation to a difference equation. To show how best to accomplish this transformation, we analyze the two terms on the right-hand side of Eq. (2.7) separately. Consider first the case of no diffusion ($\lambda \to \infty$) and $u = 1$. Equation (2.7) reduces to

$$\frac{\partial f}{\partial s} = - \frac{\partial f}{\partial x} , \tag{2.11}$$

which has the solution

$$f = \text{const} \times \delta(x - s) . \tag{2.12}$$

Now suppose that we replace Eq. (2.11) by the difference equation

$$f(l, 0, m) = f(l-1, 0, m) - (h_s/h_x) \times [f(l-1, 0, m) - f(l-1, 0, m-1)] , \tag{2.13}$$

with boundary condition

$$f(0, 0, m) = \delta_{m0} . \tag{2.14}$$

If h_s is set equal to h_x, Eq. (2.13) reduces to

$$f(l, 0, m) = f(l-1, 0, m-1) , \tag{2.15}$$

whose solution is clearly $f = \delta_{lm}$.

Thus the initial Kronecker δ function is preserved for this special choice of h_s and h_x. However, if we use $h_s \ll h_x$, [17] the form of the Kronecker δ function is not at all preserved. This is illustrated in Table I for $h_s = \frac{1}{2} h_x$. The discrepancy first appeared to be related to a well-known instability associated with numerical solutions of partial differential equations. [23] Upon converting partial differential equations such as Eq. (2.7) or the diffusion equation to difference equations it sometimes occurs that the solution grows exponentially as a function of time (here s). This disastrous result, in general, can be prevented by a correct choice of the ratio $h_s/h_x = y$. In our case we can, in fact, solve Eq. (2.13) exactly to give

$$\begin{aligned} f(l, 0, m) &= \binom{l}{m} (1-y)^{l-m} y^m, \quad l > m \\ &= 0, \qquad\qquad\qquad l < m. \end{aligned} \tag{2.16}$$

For $l = m$, we see that $f = y^m$, which grows exponentially unless $y \leq 1$. This is in fact the condition for stability. For $y = 1$, we have, of course, $f(l, 0, m) = \delta_{lm}$. In the above example, where $0 < y < 1$ for l and m large f is given by

$$f(l, 0, m) \cong \frac{1}{[2\pi l y (1-y)]^{1/2}} \times \exp\left[-(m - yl)^2 / 2ly(1-y)\right] . \tag{2.17}$$

The width of this Gaussian increases with l causing the smearing of the δ function. The problem with the choice of $h_s < h_x$ then is related not to an instability but to the special choice of the δ function boundary condition and the fact that the function varies on the same scale as the grid. In order to obtain the physically correct solution, it is necessary to take the intervals in s and x exactly equal.

One more refinement is needed to treat the first term on the right-hand side of (2.7). By the above reasoning, we need to use a different x interval for each angle to evaluate the derivatives. Thus we require

$$\Delta x = h_s \cos\theta = h_s (1 - h_u n) = h_s h_u (N_u - n) . \tag{2.18}$$

We shall use a fundamental unit $h_x = h_s h_u$, and then use a multiple of this Δx to evaluate the derivative.

TABLE I. Solution of Eq. (2.11) for $y = 0.5$.

l/m	0	1	2	3	4	5
0	1.000	0	0	0	0	0
1	0.500	0.500	0	0	0	0
2	0.250	0.500	0.250	0	0	0
3	0.125	0.375	0.375	0.125	0	0
4	0.063	0.250	0.375	0.250	0.063	0
5	0.031	0.156	0.313	0.313	0.156	0.031
6	0.016	0.094	0.234	0.313	0.234	0.094
7	0.008	0.055	0.164	0.273	0.273	0.164
8	0.004	0.031	0.109	0.219	0.273	0.219
9	0.002	0.018	0.070	0.164	0.246	0.246
10	0.001	0.010	0.044	0.117	0.205	0.246

The situation is illustrated in Fig. 2, where we see that unscattered particles traveling a path length h_s go a distance $h_s h_u(N_u - n)$ in x.

Using this result and an expression for the angular derivative we have

$$f(l, n, m) = f(l-1, n, m-N_u+n) + (h_s/\lambda h_u)\{(2-h_u n)n[f(l-1, n+1, m) + f(l-1, n-1, m) - 2f(l-1, n, m)] + (1-h_u n)[f(l-1, n+1, m) - f(l-1, n-1, m)]\}, \quad (2.19)$$

with the definition of f extended linearly outside the range $1 \leq u \leq 1$:

$$f(l, -1, m) = 2f(l, 0, m) - f(l, 1, m),$$
$$f(l, 2N_u+1, m) = 2f(l, 2N_u, m) - f(l, 2N_u-1, m). \quad (2.20)$$

The form of the angular derivative was chosen with some care and it can be verified that with the definitions in Eq. (2.20) the trapezoid-rule "integral" over u gives a vanishing result:

$$\sum_{n=0}^{N} (\nabla_u^2 f)_n h_u (1 - \tfrac{1}{2}\delta_{n0} - \tfrac{1}{2}\delta_{n, 2N_u}) = 0. \quad (2.21)$$

This is necessary to conserve electrons as Brown suggested.[17]

We now consider the stability condition on the size of h_s relative to h_u, which is another key factor in the calculation. If in Eq. (2.7) we ignore the the first term on the right-hand-side, we almost have the diffusion equation, except for the $(1-u^2)$ and the variation of λ with s. The stability criterion for the diffusion equation[23] is

$$\frac{2}{\lambda}\frac{h_s}{h_u^2} \leq 1, \quad (2.22)$$

which gives $h_s/\lambda < 0.02$ for $h_u = 0.2$. An actual calculation in which the $1-u^2$ factor is included but λ is held constant gives stability for $h_s/\lambda = 0.02$ and instability for $h_s/\lambda = 0.03$. We therefore use this criterion in our calculations.

III. SOURCE FUNCTION

The primary distribution is expressed for use in this section in a spherical-harmonic expansion:

$$f(s, \Omega, x) = \sum_l \frac{2l+1}{4\pi} F_l(s, x) P_l(\cos\theta_1), \quad (3.1)$$

with

$$F_l(s, x) = \int_0^{2\pi}\int_{-1}^{1} P_l(\cos\theta_1) f(s, \Omega_1, x) d\cos\theta_1 d\varphi_1. \quad (3.2)$$

We now briefly review the calculation,[1,5,18] in the free-electron approximation, of the secondary-electron distribution excited by a given primary electron. The probability $P_{\vec{k}\vec{K}}(\vec{k}', \vec{K}')$ per unit time for the scattering of a low-energy electron of wave vector $\vec{k}$ to a state $\vec{k}'$ by a high-energy electron of wave vector $\vec{K}$ scattering to a state $\vec{K}'$ is given by the golden-rule expression

$$P_{\vec{k}\vec{K}}(\vec{k}', \vec{K}') = \frac{2\pi}{\hbar} |\langle \vec{k}'\vec{K}' | H_{\rm int} | \vec{k}\vec{K}\rangle|^2 \delta_{\vec{k}+\vec{K}, \vec{k}'+\vec{K}'} \times \delta(E_{\vec{K}} + E_{\vec{k}} - E_{\vec{K}'} - E_{\vec{k}'}). \quad (3.3)$$

Representing the electron states by wave functions of the form $\psi_{\vec{K}}(\vec{R}) = e^{i\vec{K}\cdot\vec{R}}/V^{1/2}$, with V the volume of the sample, and assuming a screened Coulomb interaction

$$H_{\rm int} = e^2 e^{-\alpha|\vec{R}-\vec{r}|}/|\vec{R}-\vec{r}|, \quad (3.4)$$

one obtains

$$P_{\vec{k}\vec{K}}(\vec{k}', \vec{K}') = \frac{32\pi^3 e^4}{\hbar V^2(|\vec{K}'-\vec{K}|^2+\alpha^2)} \times \delta(E_{\vec{K}} + E_{\vec{k}} - E_{\vec{K}'} - E_{\vec{k}'})\, \delta_{\vec{k}', \vec{k}+\vec{K}'-\vec{K}}, \quad (3.5)$$

where e is the electronic charge. We now calculate the number of electrons per unit time excited into the state $\vec{k}'$ by the initial primary in state $\vec{K}$. Assuming $\alpha = 0$, this is

$$P_{\vec{K}\vec{k}'} = \sum_{\vec{k}\vec{K}'} P_{\vec{k}\vec{K}}(\vec{k}', \vec{K}') = \frac{8\pi m e^4}{\hbar^3 V} \times \frac{K^2 k'^2 - (\vec{k}'\cdot\vec{K})^2 - (k'^2 - k_F^2)|\vec{K}-\vec{k}'|^2}{|\vec{K}-\vec{k}'|^3 (k_p'^2 - k_F^2)^2} \quad (3.6)$$

for

$$\vec{k}'\cdot(\vec{K}-\vec{k}') \leq k_F|\vec{K}-\vec{k}'| \quad (3.7)$$

and is otherwise zero. Here $k_F(E_F)$ is the Fermi momentum (energy). If we average $P_{\vec{K}\vec{k}'}$ over the secondary angle $\theta_2 = \theta_{\vec{k}', \vec{K}}$ we obtain[1]

$$\bar{P}_{\vec{K}\vec{k}'} = \frac{8\pi m e^4}{\hbar^3 K V} \frac{2}{3}\frac{k_F^3}{k'} \frac{1}{(k'^2 - k_F^2)^2}. \quad (3.8)$$

Following Stoltz[5] we consider Eq. (3.7) in the limit that $K \gg k' > k_F$, and the result is simply Eq. (3.8) with the $\frac{2}{3}$ replaced by $\sin^2\theta_2$.[24]

Let us now consider the distribution of secondary electrons per unit volume per unit energy and solid angle $\Omega_2 = (\theta_2, \varphi_2)$ per unit density of primary electrons. We thus divide the above result by $1/V$, the primary density, and multiply by $(1/8\pi^3)k'^2 dk'/dE'$ to obtain

$$S(E', \Omega_2) = \left(\frac{2}{m\mathcal{E}}\right)^{1/2} \frac{e^4 k_F^3}{8\pi^2 (E'-E_F)^2} \sin^2\theta_2. \quad (3.9)$$

Expanding now in spherical harmonics we have

$$S(E', \Omega_2) = \sum_l (2l+1)/4\pi\, S_l(E') P_l(\cos\theta_2), \quad (3.10)$$

with

$$S_0(E') = \left(\frac{2}{m\mathcal{E}}\right)^{1/2} \frac{e^4 k_F^3}{3\pi(E'-E_F)^2}, \quad (3.11a)$$

$$S_2(E') = -S_0(E')/5, \quad (3.11b)$$

$$S_l(E') = 0, \quad l \neq 0, 2 . \tag{3.11c}$$

We now multiply Eq. (3.9) or (3.10) by the primary distribution function [Eq. (3.1)] and integrate over $\vec{K}$ to obtain the total rate of production of secondaries per unit volume, energy, and solid angle:

$$\bar{S}(E', \Omega, x) = \int S(E', \Omega_2) f(s, \Omega_1, x) K^2 dK d\Omega_1$$
$$= \int \sum_l \frac{2l+1}{4\pi} S_l(E') P_l(\cos\theta_2) \sum_{l'} \frac{2l'+1}{4\pi}$$
$$\times F_{l'}(s, x) P'_l(\cos\theta_1) K^2 dK d\Omega_1 . \tag{3.12}$$

Here $\Omega = (\theta, \varphi)$ gives the orientation of the secondary-electron velocity with respect to the inward normal. We now make use of the addition theorem for spherical harmonics[25]

$$P_l(\cos\theta_2) = P_l(\cos\theta) P_l(\cos\theta_1)$$
$$+ 2 \sum_{m=1}^{l} \frac{(l-m)!}{(l+m)!} P_l^m(\cos\theta) P_l^m(\cos\theta_1) \cos m(\theta - \theta_1) , \tag{3.13}$$

where the P_l^m are associated Legendre functions, to obtain

$$\bar{S}(E', \theta, x) = \sum_l \frac{2l+1}{4\pi} P_l(\cos\theta)$$
$$\times \int S_l(E') F_l(s, x) K^2 dK , \tag{3.14}$$

where the φ variable is suppressed in this equation and those that follow due to azimuthal symmetry. Then

$$S(E', \theta, x) = \frac{m e^4 k_F^3}{6\pi^2 \hbar^3 (E' - E_F)^2}$$
$$\times [A_0(x) - A_2(x) P_2(\cos\theta)] , \tag{3.15}$$

with

$$A_l(x) = \int_0^{\mathcal{E}_{\max}} F_l(\mathcal{E} x) d\mathcal{E} . \tag{3.16}$$

IV. SECONDARY TRANSPORT

In this section we derive the observed current due to the secondary-electron source function obtained in Sec. III. According to Wolff's[19] work, the Boltzmann equation for the secondary transport can be written as[1]

$$-v\cos\theta \frac{\partial N(E, \theta, x)}{\partial x} = \bar{S}(E, \theta, x)$$
$$- \frac{v}{\lambda_0(E)} N(E, \theta, x) + \int N(E', \theta', x) \frac{v}{\lambda_0(E')}$$
$$\times P(E, E', \cos\Theta) dE' d\Omega' , \tag{4.1}$$

where $\lambda_0(E)$ is the mean free path of a secondary electron with energy E, v is its velocity, and $p(E, E'\cos\Theta)$ is the probability for a spherically symmetric scattering potential that, given an electron in the state E', there will be an electron in the state E after collision. Here Θ is the angle between the velocities in the two states. Using the expansions

$$N(E, \theta, x) = \sum_l \frac{2l+1}{4\pi} N_l(E, x) P_l(\cos\theta) , \tag{4.2}$$

$$P(E, E', \cos\Theta) = \sum_l \frac{2l+1}{4\pi} p_l(E, E') P_l(\cos\Theta) , \tag{4.3}$$

$$\bar{S}(E, \theta, x) = \sum_l \frac{2l+1}{4\pi} \bar{S}_l(E, x) P_l(\cos\theta) , \tag{4.4}$$

we obtain the system of equations

$$-\lambda_0(E) \left(\frac{l}{2l+1} \frac{\partial \psi_{l-1}(E, x)}{\partial x} \right.$$
$$\left. + \frac{l+1}{2l+1} \frac{\partial \psi_{l+1}(E, x)}{\partial x} \right) = -\psi_l(E, x) + \bar{S}_l(E, x)$$
$$+ \int_E^\infty \psi_l(E', x) p_l(E, E') dE' \tag{4.5}$$

for the functions

$$\psi(E, \theta, x) = \sum_l \frac{2l+1}{4\pi} \psi_l(E, x) P_l(\cos\theta) ,$$
$$\psi_l(E, x) = \frac{v}{\lambda_0(E)} N_l(E, x) . \tag{4.6}$$

If it is further assumed that the scattering is spherically symmetric in the center-of-mass system and that the metal's electrons are at rest before collision, we have[19]

$$P(E, E', \cos\Theta) = \frac{2}{\pi} \cos\Theta \, \delta(E - E'\cos^2\Theta) \tag{4.7}$$

and hence

$$p_l(E, E') = \frac{2}{E'} P_l \left[\left(\frac{E}{E'} \right)^{1/2} \right] . \tag{4.8}$$

These equations are to be solved in a semi-infinite medium, with a boundary condition corresponding to specular reflection at the surface. This can be written for $0 < \theta < \frac{1}{2}\pi$ as

$$\psi(E, \theta, 0) = R(E, \pi - \theta) \psi(E, \pi - \theta, 0) , \tag{4.9}$$

where R is the reflection coefficient discussed at the end of this section.

The complete solution is very difficult, and we have not obtained it. Wolff[19] solved the equation for an isotropic monoenergetic source function which is homogeneous within the half-space occupied by the metal. Stoltz[5] considered a spatially homogeneous anisotropic source function given by Eq. (3.15) with $A_0 = A_2 = 1$.

In this paper we first outline the calculation for a spatially homogeneous but anisotropic source function. This results in a source induced P_0-

and P_2-type anisotropy. We then use that solution and the full equation in a perturbative manner to find a P_1-type anisotropy which is induced by the spatial variation of A_0 and A_1.

The above ignores the boundary condition [Eq. (4.9)]. We shall indicate a method of using the solutions of the homogeneous equation [Eqs. (4.30) below] to fit the results to the boundary conditions. Rather than carry this through, however, we obtain an alternative result for the P_1 anisotropy from the boundary condition alone.

With the neglect of spatial derivatives, and the use of Eq. (4.8), Eq. (4.5) may be written

$$\psi_l(E) = \bar{S}_l(E) + 2\int_E^\infty \psi_l(E')\, P_l\left[\left(\frac{E}{E'}\right)^{1/2}\right]\frac{dE'}{E'} \,. \tag{4.10}$$

The relevant Green's functions are then defined by

$$G_l(E, E_0) = \delta(E - E_0) + 2\int_E^\infty G_l(E', E_0) P_l\left[\left(\frac{E}{E'}\right)^{1/2}\right]\frac{dE'}{E'} \,, \tag{4.11}$$

where the first few Green's functions can be obtained as

$$E_0 \geq E\colon\ G_0(E, E_0) = \frac{2E_0}{E^2} + \delta(E - E_0) \,, \tag{4.12a}$$

$$G_1(E, E_0) = \frac{2E_0^{1/2}}{E^{3/2}} + \delta(E - E_0) \,, \tag{4.12b}$$

$$G_2(E, E_0) = \frac{2}{(EE_0)^{1/2}} \times\cos\left[\frac{\sqrt{3}}{2}\ln\left(\frac{E_0}{E}\right)\right] + \delta(E - E_0) \,, \tag{4.12c}$$

$$E_0 \leq E\colon\ G_l(E, E_0) = 0 \,. \tag{4.12d}$$

The ψ functions are given by

$$\psi_l(E) = \int_{E_F}^{E_m} G_l(E, E_0)\, \bar{S}_l(E_0) dE_0 \,, \tag{4.13}$$

where E_m is a maximum energy ~ 100 eV such that the assumptions made in deriving Eq. (4.5) are true. Using Eqs. (4.12), (4.13), and (3.15), and assuming $\lambda_0(E) = \lambda_0$, one then obtains

$$\psi'(E, x) = \frac{1}{4\pi}\,\psi_0(E, x) + \frac{5}{4\pi}\,\psi_2(E, x) P_2(\cos\theta) \,, \tag{4.14}$$

$$\psi_0(E, x) = \frac{\gamma}{\lambda_0(E)}\left(\frac{2}{m}\right)^{1/2} \alpha A_0(x) \,, \tag{4.15}$$

$$\psi_2(E, x) = -\frac{\gamma}{5\lambda_0(E)}\left(\frac{2}{m}\right)^{1/2} \beta A_2(x) \,, \tag{4.16}$$

where

$$\gamma = \frac{2m}{\hbar^3}\left(\frac{(2m)^{1/2}\lambda_0 e^4 k_F^3}{6\pi}\right) \,, \tag{4.17}$$

$$\alpha = \frac{2}{E^2}\left[\ln\left(\frac{E_m - E_F}{E - E_F}\right) + E_F\left(\frac{1}{E - E_F} - \frac{1}{E_m - E_F}\right)\right] + \frac{1}{(E - E_F)^2} \,, \tag{4.18}$$

$$\beta = \frac{2}{E^2}\sum_{n=0}^{\infty} T(n)\left[\left(\frac{E}{E_m}\right)^{3/2}\left(\frac{E_F}{E_m}\right)^n \times\left(\frac{\sqrt{3}}{2n+3}\, S - C\right) + \left(\frac{E_F}{E}\right)^n\right] + \frac{1}{(E - E_F)^2} \,, \tag{4.19}$$

with

$$T(n) = \frac{2(2n+3)(n+1)}{(2n+3)^2 + 3} \,, \tag{4.20}$$

$$S = \sin\left[\frac{\sqrt{3}}{2}\ln\left(\frac{E_m}{E}\right)\right] \,, \tag{4.21}$$

$$C = \cos\left[\frac{\sqrt{3}}{2}\ln\left(\frac{E_m}{E}\right)\right] \,. \tag{4.22}$$

Since $\bar{S}_1(E) = 0$, the derivatives of (4.15) and (4.16) serve as the sole source for a $\psi_1(E)$ term in the $l = 1$ member of Eqs. (4.5). That term is then given by

$$\psi_1(E, x) = \int_{E_F}^{E_m} G_1(E, E_0)\, \bar{S}_1^{\mathrm{EFF}}(E_0, x) dE_0 \,, \tag{4.23}$$

with

$$\bar{S}_1^{\mathrm{eff}}(E_0, x) = \frac{\gamma}{3}\left(\frac{2}{m}\right)^{1/2}\left[\alpha(E_0) B_0(x) - \tfrac{2}{5}\,\beta(E_0) B_2(x)\right], \tag{4.24}$$

where

$$B_l(x) = \frac{dA_l(x)}{dx} \,. \tag{4.25}$$

Then

$$\psi_1(E, x) = \frac{\gamma}{3}\left(\frac{2}{m}\right)^{1/2}\left[J_0(E) B_0(x) - \tfrac{2}{5} J_2(E) B_2(x)\right] \tag{4.26}$$

and

$$\psi''(E, \theta, x) = \frac{1}{4\pi}\,\psi_0(E, x) + \frac{3}{4\pi}\,\psi_1(E, x) P_1(\cos\theta) + \frac{5}{4\pi}\,\psi_2(E, x) P_2(\cos\theta), \tag{4.27}$$

where

$$J_0(E) = \frac{2}{E^{2/3}}\left[\frac{1}{E_m - E_F}\left(-\frac{5E_F}{E^{1/2}} + 3E_m^{1/2}\right) + \frac{1}{E - E_F}\left(\frac{5E_F}{E^{1/2}} - 3E^{1/2}\right) + \frac{3}{2E_f^{1/2}}\ln\left(\frac{(E^{1/2} - E_F^{1/2})(E_m^{1/2} + E_F^{1/2})}{(E^{1/2} + E_F^{1/2})(E_m^{1/2} - E_F^{1/2})}\right) - \frac{5}{E^{1/2}}\ln\left(\frac{E - E_F}{E_m - E_F}\right)\right] + \frac{1}{(E - E_F)^2} \tag{4.28}$$

and

$$J_2(E) = \beta(E) + \frac{2}{E^{3/2}}$$

$$\times\Bigg[\sum_{n=0}^{\infty} T(n)\Bigg(\frac{2E_F^n}{n+1/2}\Bigg(\frac{1}{E^{n+1/2}}-\frac{1}{E_m^{n+1/2}}\Bigg)+\frac{8}{7E_m^{1/2}}\left(\frac{E_F}{E_m}\right)^n\Bigg\{\frac{\sqrt{3}}{2n+3}\Bigg[-\frac{ES}{E_m}+\frac{\sqrt{3}}{2}\left(1-\frac{EC}{E_m}\right)\Bigg]-1+\frac{EC}{E_m}+\frac{\sqrt{3}}{2}\frac{ES}{E_m}\Bigg\}\Bigg)+\frac{E^{1/2}}{E-E_F}-\frac{E_m^{1/2}}{E_m-E_F}+\frac{1}{2E_f^{1/2}}\times\ln\left(\frac{(E_m^{1/2}-E_F^{1/2})(E^{1/2}+E_F^{1/2})}{(E_m^{1/2}+E_F^{1/2})(E^{1/2}-E_F^{1/2})}\right)\Bigg]\ . \tag{4.29}$$

Thus far no account has been taken of the boundary condition [Eq. (4.9)]. In principle, a means of solving this problem is to add to our result the solutions of the homogeneous equation, i.e., Eq. (4.5), with $S_l = 0$. If we further ignore the spatial derivative of ψ, those solutions are

$$l=0:\quad \psi_0^H \propto E^{-2}\ , \tag{4.30a}$$

$$l=1:\quad \psi_1^H \propto E^{-3/2}\ , \tag{4.30b}$$

$$l=2:\quad \psi_2^H \propto E^{-1/2\pm i3/2}\ . \tag{4.30c}$$

Using a more approximate approach, we keep the P_0 and P_2 terms as those induced by the anisotropic source terms and determine an alternative P_1 term, ψ_1', from the boundary condition. In fact, we choose ψ_1' to satisfy the weaker condition

$$\psi(E,\ 0,\ 0) = R(E,\ \pi)\,\psi(E,\ \pi,\ 0)\ . \tag{4.31}$$

This is used to determine ψ_1' in

$$\psi'''(E,\ 0,\ x) = \frac{1}{4\pi}\,\psi_0(E,\ x) + \frac{3}{4\pi}\,\psi_1'(E,\ x)P_1(\cos\theta) + \frac{5}{4\pi}\,\psi_2(E,\ x)P_2(\cos\theta) \tag{4.32}$$

in a straightforward manner. Now if this is to be a solution of the complete system (still neglecting spatial derivatives) for ψ_1, then we should have

$$\psi_1' = \psi_1 + \psi_1^H\ , \tag{4.33}$$

where ψ_1^H is a solution of the homogeneous equation, i.e., $\propto E^{-3/2}$. We shall compare the results below.

If the metal is represented by the Sommerfeld well of depth $W = 12$ eV shown in Fig. 3, the reflection coefficient for electrons incident from the inside is given by

$$R(E,\ \bar\theta) = \left(\frac{(E_\perp)^{1/2}-(E_\perp')^{1/2}}{(E_\perp)^{1/2}+(E_\perp')^{1/2}}\right)^2\ , \tag{4.34}$$

where the components of energy along the surface normal are defined in the figure,

$$E_\perp = E\cos^2\bar\theta\ , \tag{4.35}$$

$$E_\perp' = E\cos^2\bar\theta - W\ , \tag{4.36}$$

and $\bar\theta = \pi - \theta$ is the angle which the electron's velocity makes with the outward normal. (We note that our simple model of the surface potential somewhat overestimates the reflection.[26] This error is not of fundamental importance here.) The transmission coefficient $T = 1 - R$ and thus

$$T(E,\ \bar\theta) = \frac{4E(E\cos^2\bar\theta - W)^{1/2}\cos\bar\theta}{E^{1/2}\cos\bar\theta + (E\cos^2\bar\theta - W)^{1/2}}\ . \tag{4.37}$$

The current observed outside the sample is given in terms of $N(E,\ \theta,\ x)$ as follows. The current incident on the surface j_s^i is

$$j_s^i(E,\ \bar\theta)dE\,d\bar\varphi\,d\cos\bar\theta = T(E,\ \bar\theta)N(E,\ \pi-\bar\theta,\ 0) \times v\cos\bar\theta\,dE\,d\bar\varphi\,d\cos\bar\theta\ . \tag{4.38}$$

By continuity, the current outside j_s^0 is then given by

$$j_s^0 dE'\,d\varphi\,d\cos\theta' = j_s^i\,dE\,d\bar\varphi\,d\cos\bar\theta\ . \tag{4.39}$$

But $dE = dE'$, $d\bar\varphi = d\varphi'$, and from the refraction law we have

$$v\sin\bar\theta = v'\sin\theta'\ , \tag{4.40}$$

$$\frac{d\cos\bar\theta}{d\cos\theta'} = \frac{E'\cos\theta'}{E\cos\bar\theta}\ , \tag{4.41}$$

where θ' is the angle that the secondary electron makes with the outward surface normal after passing through the barrier. Then

$$j_s^0(E',\ \theta') = N(E,\ \pi-\theta,\ 0)\,v\,(E'/E)\cos\theta' \tag{4.42}$$

and

$$\frac{j_s^0(E',\ \theta')}{j_s^0(E',\ 0)} = \frac{T(E,\ \bar\theta)N(E,\ \pi-\theta,\ 0)\cos\theta'}{T(E,\ \bar\theta)\,N(E,\ \pi,\ 0)}\ . \tag{4.43}$$

Thus as $E' \to 0$, Eq. (4.43) yields

$$\frac{j_s(0,\ \theta')}{j_s^0(0,\ 0)} = \cos\theta'\ . \tag{4.44}$$

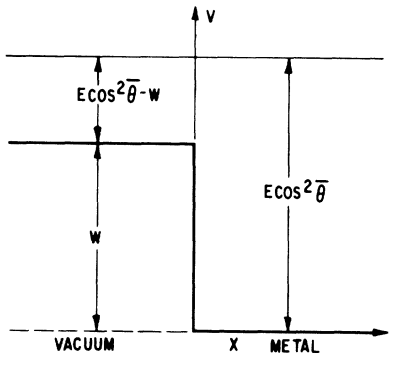

FIG. 3. Potential as a function of distance in the region near the metal surface.

TABLE II. Parameters used in calculation of primary distribution.

E_{max}(keV)	2	10
h_u	0.2	0.2
ρh_x (g cm)	0.13×10^{-7}	0.24×10^{-6}
ρh_s (g cm)	0.65×10^{-7}	1.2×10^{-6}
ρR (g cm)	2.31×10^{-5}	3.57×10^{-4}
l_{max}	356	298

We next consider the total number of electrons emitted with a given energy. That energy distribution of observed electrons is given by

$$j_s^0(E') = \int_{\cos\bar\theta_e}^1 j_s^0(E', \bar\theta)\, d\bar\varphi\, d\cos\bar\theta$$
$$= 2\pi v \int_{\cos\bar\theta_e}^1 T(E, \bar\theta) N(E, \pi-\bar\theta, 0)\cos\bar\theta\, d\cos\bar\theta\,, \tag{4.45}$$

where $\bar\theta_e$ is the maximum angle [given by Eq. (4.40) as $\arccos(W/E)$] for which electrons can pass through the surface. Using Eq. (4.2) we obtain

$$j_s^0(E') = v\sum_l \frac{2l+1}{2} N_l(E, 0) M_l\,, \tag{4.46}$$

where

$$M_l = \int_{\cos\theta_e}^1 T(E, \bar\theta) P_l(\cos(\pi-\theta))\cos\bar\theta\, d\cos\bar\theta\,. \tag{4.47}$$

We normalize this current to unit incident primary flux. The primary flux F is

$$F = v\,\frac{\Delta u}{2}\, h_s\, \frac{\partial \mathcal{E}}{\partial s}\, \frac{k^2 dk}{d\mathcal{E}}\cos\theta_1\,, \tag{4.48}$$

where

$$\frac{k^2 dk}{d\mathcal{E}} = \frac{m^{3/2}(2\mathcal{E})^{1/2}}{\hbar^3} \tag{4.49}$$

and $\partial\mathcal{E}/\partial s$ is given by Eq. (2.5). When A_0 and A_2 are taken to be equal to one, as in Stoltz's calculation, the flux which must be used in the normalization is

$$F^s = \hbar K\cos\theta_1/m\,. \tag{4.50}$$

V. RESULTS

The primary-electron distributions were calculated from the difference equation [Eq. (2.19)] for three cases: 2- and 10-keV electrons normally incident on the sample, and 10-keV electrons incident at $\theta_1 \sim 53°$ for which $\cos\theta_1 = 0.6$. The parameters used are shown in Table II. We calculate f for $s = h_s(l+1)$ from the angular and spatial distribution for $s = h_s(l)$. The starting values of f for normal incidence are

$$2\pi f(0, n, m) = \delta_{n0}\delta_{m0} + 2\delta_{n,-1}\delta_{m0}\,. \tag{5.1}$$

Notice that we have included the linear extrapolation [Eq. (2.20)] in n. To ensure that the boundary condition [Eq. (2.9)] is satisfied we require

$$f(l, n, -1) = 0, \quad 0 \le n \le 5, \quad l > 0. \tag{5.2}$$

For the 53° case we consider an annular source of electrons in order to preserve azimuthal symmetry. This is obtained by using the initial distribution

$$2\pi f(0, n, m) = \tfrac{1}{2}\delta_{n2}\delta_{m0} \tag{5.3}$$

together with the condition in Eq. (5.2). The factor $\frac{1}{2}$ is included to make the normalization of this "two-sided δ function" the same as that at $n = 0$ which is "one sided." The secondary emission resulting from the annular source corresponds to the azimuthal average of that due to a beam coming in at a fixed angle. The resultant pure energy distributions are therefore the same as for oblique incidence.

Due to the computing time limitations imposed by the stability conditions we integrated the equations down only to about $\frac{3}{4}$ of the initial energy and used a linear extrapolation of quantities of interest for the rest of the range. Also, due to the choice of x intervals in Eq. (2.18), it was appropriate to calculate instead of f,

$$\bar f(l, n, m_0+2) = \sum_{m=m_0}^{m_0+M-1} f(l, n, m)\,, \tag{5.3a}$$

where $m = 5$ for normal incidence and $m = 3$ for the 53° case.

f is now expanded in spherical harmonics. F_0, the distribution function integrated over angle, is plotted in Fig. 4 for 10-keV normally incident electrons, where the bar notation will not be used in what follows. The insert shows the detailed shape of the tail of the distribution and the linear extrapolation used to evaluate results given below. These results are very similar to the results of a Monte Carlo calculation by Green.[16]

Figures 5 and 6 show the F_1 and F_2 components for 10-keV normally incident electrons. We see that for $s = x$ they are as large as the F_0 component. This is due to the initial angular δ function. However, the higher components decay more rapidly as a function of energy. It is interesting to note that the current, which is proportional to F_1, is going into the sample for higher energies (shorter path) in each plot but is going out at lower energies. The results for the 2-keV normally incident electron were similar to those the of 10-keV case.

Figure 7 shows the density of primaries relative to the initial beam density

$$\frac{\rho(x)}{\rho_0} = \int_0^{\mathcal{E}_{max}} F_0\,\mathcal{E}^{1/2}\, \frac{d\mathcal{E}}{\mathcal{E}_{max}^{1/2}\, 0.1\, h_s (d\mathcal{E}/ds)_{\mathcal{E}_{max}}} \tag{5.4}$$

for the 2-keV and 10-keV normally incident elec-

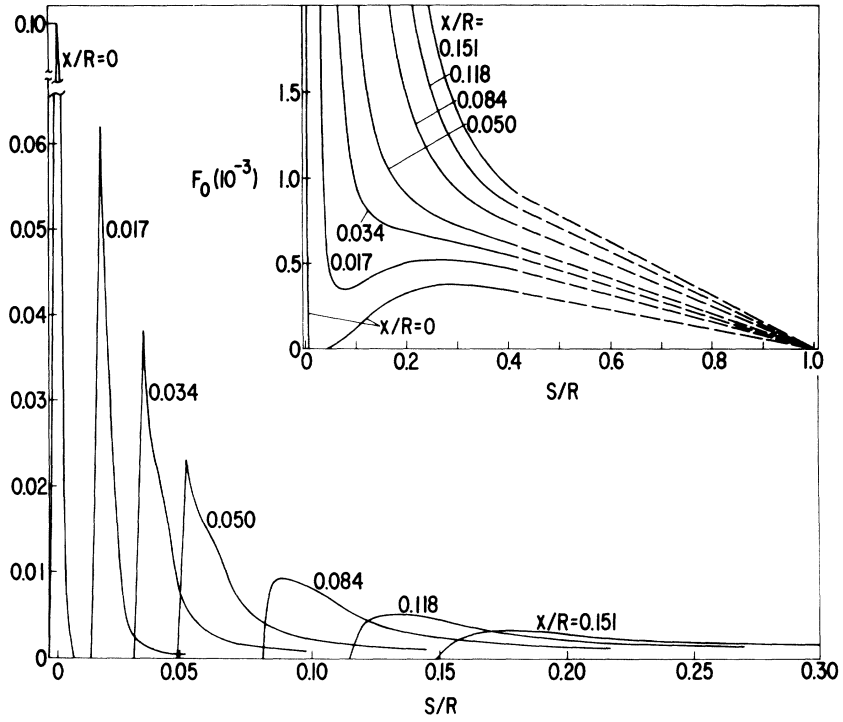

FIG. 4. F_0, the coefficient of the $l=0$ term of a Legendre expansion of the primary-electron density, associated with a normally incident 10-keV beam, as a function of the path length traversed s. The various curves correspond to the coefficient at various distances from the surface. In the insert is a magnification of the tail of the distribution showing (dashed lines) the extrapolations used in obtaining energy integrals of the coefficient. Lengths are given in units of the total range R, and units of F_0 are defined by Eqs. (5.1), (5.3a), and (3.2).

tron and the 10-keV electron incident at $\theta_1 = 53°$.

In Fig. 8(a) we show the results of a calculation of the fractional distribution of the total number of backscattered electrons which is given by

$$\frac{d\eta}{d(\mathcal{E}/\mathcal{E}_{\max})} = \frac{\mathcal{E}F_1(\mathcal{E})}{0.1h_s(d\mathcal{E}/ds)_{\mathcal{E}_{\max}}} . \tag{5.5}$$

Figure 8(b) shows the experimental results of

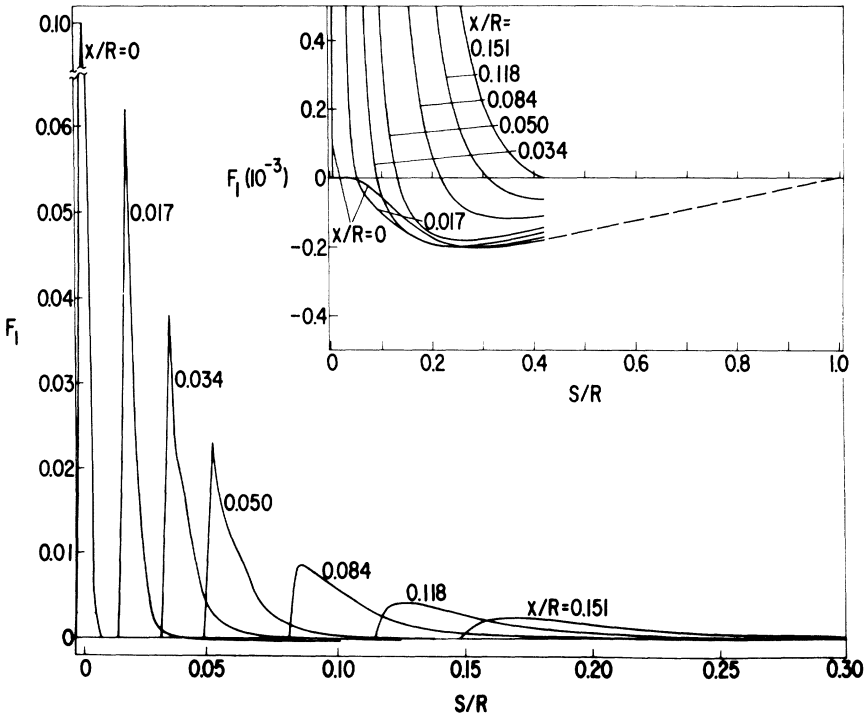

FIG. 5. F_1, the coefficient of a Legendre expansion of the primary-electron density, associated with a normally incident 10-keV beam, as a function of the path length traversed s. The various curves correspond to the coefficient at various distances from the surface. In the insert is a magnification of the tail of F_1, showing (dashed line) the extrapolation used in obtaining energy integrals of the coefficient. Lengths are given in units of the total range R, and units of F_1 are defined by Eqs. (5.1), (5.3a), and (3.2).

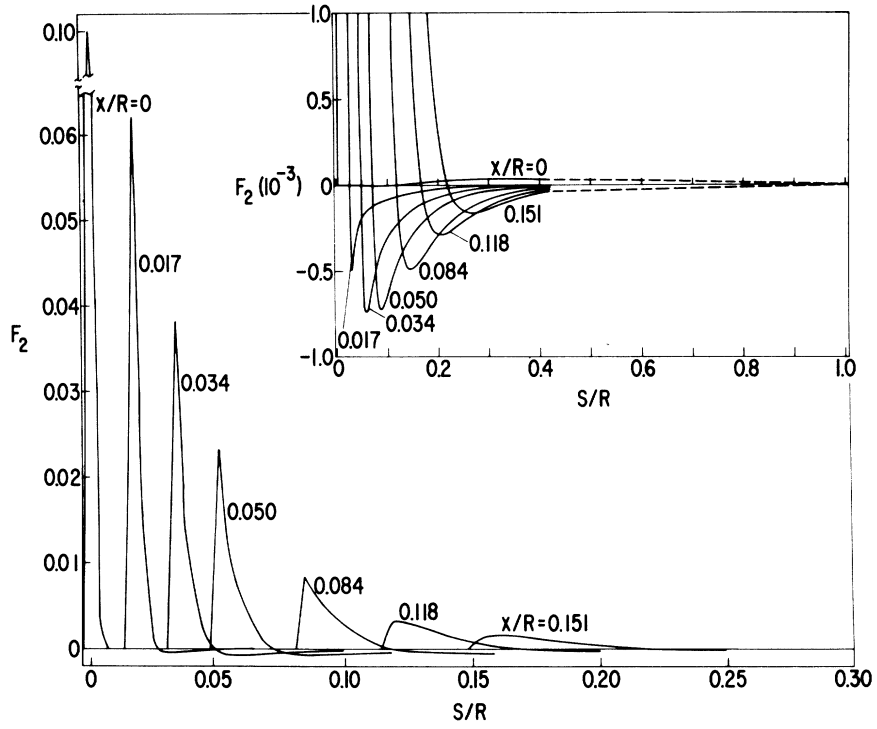

FIG. 6. F_2, the coefficient of the $l=2$ term of a Legendre expansion of the primary-electron density, associated with a normally incident 10-keV beam, as a function of the path length traversed s. The various curves correspond to the coefficient at various distances from the surface. In the insert is a magnification of the tail of F_2, showing (dashed lines) the extrapolation used in obtaining energy integrals of the coefficient. Lengths are given in units of the total range R, and units of F_2 are defined by Eqs. (5.1), (5.3a), and (3.2).

Darlington[27] for Cu with $\mathcal{E}_{max}=30$ keV as measured at two different angles with respect to the normally incident beam. The normalization for these curves has been obtained from Bishop's[28] experimental determination of the total backscatter fraction η. For $\mathcal{E}_{max} > 5$ keV, these results are relatively independent of $\mathcal{E}_{max}$. The dotted curve in the figure shows Brown's[17] calculated results for the fractional distribution of the total number of backscatttered electrons for Cu with $\mathcal{E}_{max}=29$ keV. The peak position of the 10-keV $\theta=0$ curve in Fig. 8(a) is somewhat closer to that of the experimental curves than the peak position obtained by Brown. Both diffusion calculations yield curve shapes which agree better with experiment than that obtained in the Monte Carlo calculation shown in the figure. Table III shows the total backscatter fraction obtained in some previous calculations and experiments. Our results are in accord with this work. The total backscatter coefficient exhibits a dependence on the angle of incidence (as

TABLE III. Backscatter fraction (η).

Energy (keV)	Angle of incidence (deg)	This work	Monte Carlo[a]	Brown[b]	Expt.
2	0	0.33			
5	0				0.35[c]
10	0	0.29			0.33[c]
10	53	0.47			
29	0		0.30	0.29	0.30[d], 0.32[c]
29	45		0.37		0.44[d]
29	67.5		0.50		

[a]Reference 29.
[b]Reference 17.
[c]Reference 28.
[d]Reference 16.

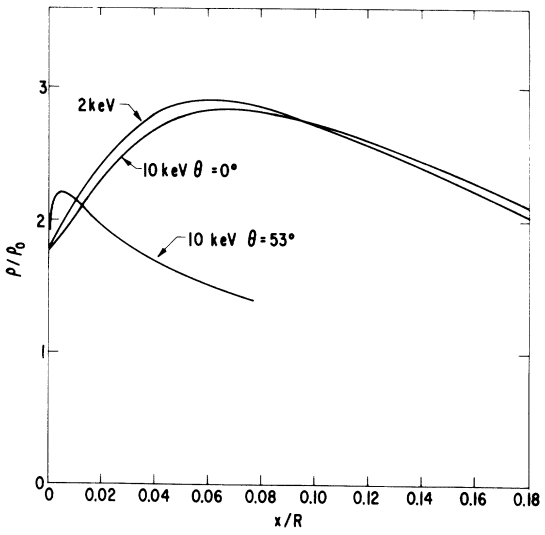

FIG. 7. Total density of primary electrons relative to the initial beam density [Eq. (5.4)] as a function of distance x from the surface. The distance is given in units of the total range R.

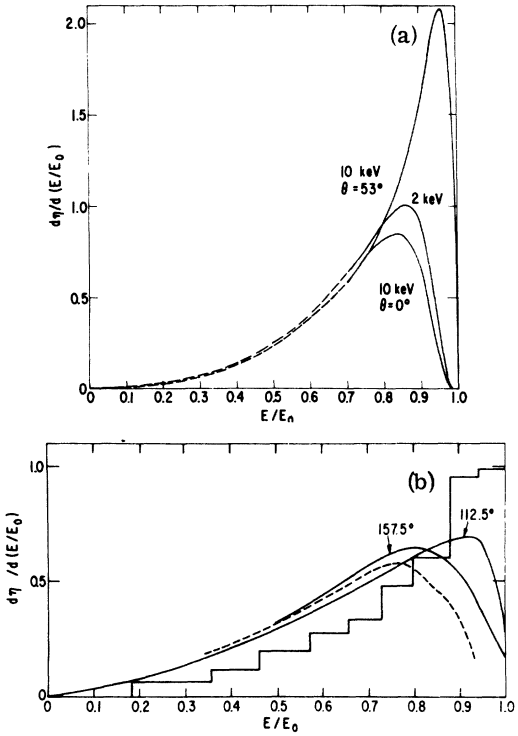

FIG. 8. Fractional distribution of backscattered electrons as a function of energy. (a) This work; the dashed portions of the curves are calculated using the extrapolation shown in Fig. 5. The angles are angles of incidence. (b) The dashed curve shows Brown's calculation; the solid curves—Darlengton's experimental results, and the histogram—Bishop's Monte Carlo calculation. These are all for normal incidence; the angles shown are the angles of observation.

far as we have calculated it) in line with the experimental results of Green[16] and the Monte Carlo calculations[29], while the energy dependence is in agreement with Bishop's[28] results.

The coefficients A_0 and A_2 characterizing the source function for the secondary electrons are given as a function of position in Figs. 9 and 10 for the 2- and 10-keV cases, respectively. As described in Sec. IV, we next calculated ψ_0 and ψ_2, [Eqs. (4.15) and (4.16)] for the distribution function ψ' [Eq. (4.14)]. Here we are neglecting both the spatial dependence of the source function, and the boundary condition. ψ_0 and ψ_2 are shown as a function of energy in Figs. 11 and 12 for the 2- and 10-keV cases, respectively. We next calculated ψ_1 and ψ_1', in the first of which we neglect the boundary but include the spatial inhomogeneity approximately, and in the second of which we approximate the boundary conditions but neglect the inhomogeneity. The secondary-electron mean free path is taken to be 20 Å.[30] These results are also given in Figs. 11 and 12. We see that for the 2-keV case there is a considerable difference between ψ_1 and ψ_1', which appears to be the consequence of the considerable variation of the source function in a secondary-electron mean free path. In the 10-keV case, the source function varies less, and the difference is smaller. It is also evident that ψ'' becomes negative for $\theta > \frac{1}{2}\pi$ because of the large value of ψ_1 for this case, a weakness of the calculation. The difference between ψ_1 and ψ_1' com-

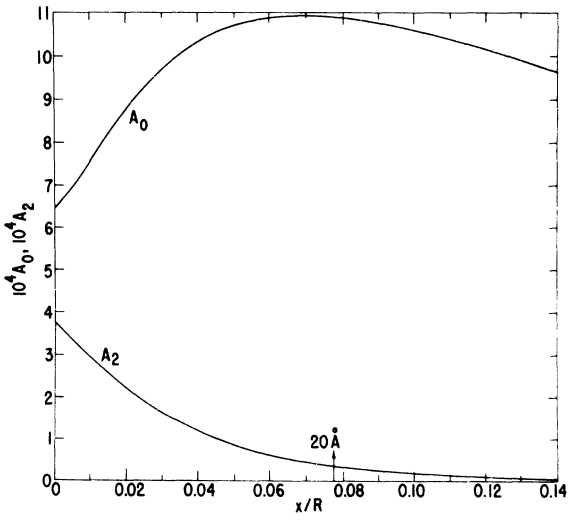

FIG. 9. Coefficients A_0 and A_2, for 2-keV normally incident primary electrons, as a function of distance x from the surface. Lengths are given in units of the total range R, and units of A_0 and A_2 are defined by Eq. (3.16) with E in eV.

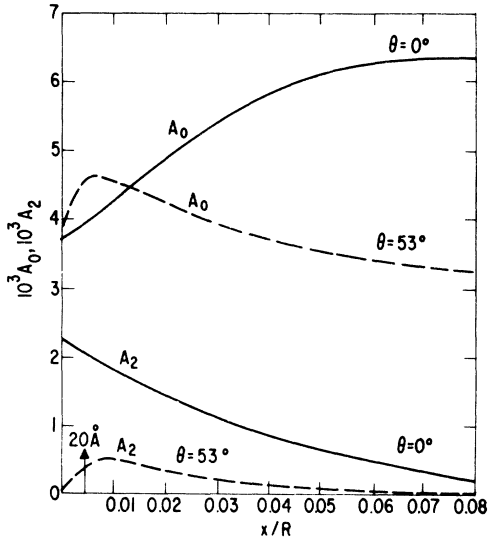

FIG. 10. Coefficients A_0 and A_2 for 10-keV normally incident primary electrons and for 10-keV primary electrons incident at an angle of 53°, as a function of distance x from the surface. Lengths are given in units of the total range R, and units of A_0 and A_2 are defined by Eq. (3.16) with E in eV.

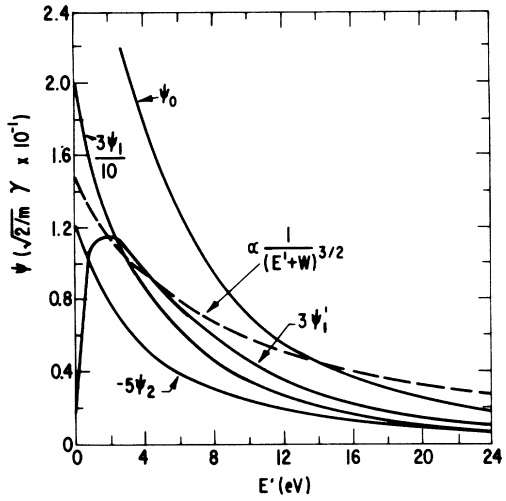

FIG. 11. Coefficients of a Legendre expansion of the secondary-electron density at the surface due to a 2-keV normally incident primary-electron beam as a function of secondary-electron energy with respect to the vacuum level.

pares reasonably with the $E^{-3/2}$ solution of the homogeneous equation for $l=1$ in which the spatial inhomogeneity terms have also been neglected, and which is also plotted.

The above results were used to calculate the secondary-electron current outside the surface. To study the angular dependence we plot

$$P = \frac{j_s^0(E,\theta')}{j_s^0(E,0)} - \cos\theta' \qquad (5.6)$$

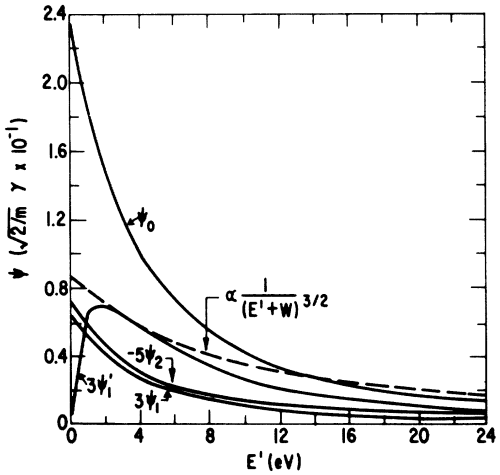

FIG. 12. Coefficients of a Legendre expansion of the secondary-electron density at the surface due to a 10-keV normally incident primary-electron beam as a function of secondary-electron energy with respect to the vacuum level.

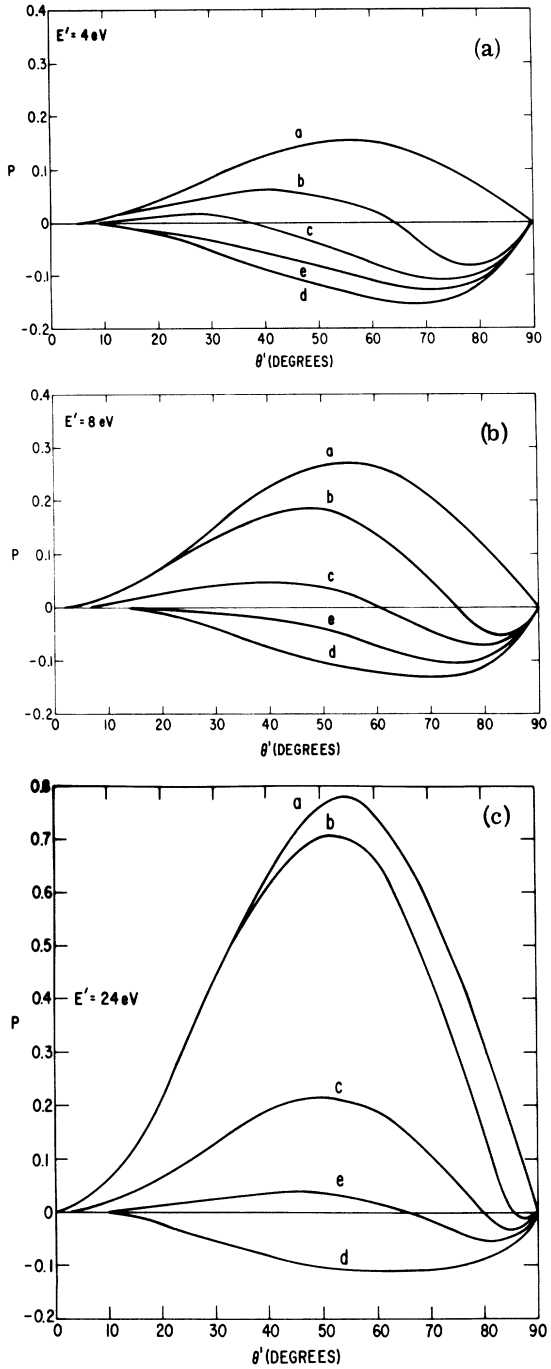

FIG. 13. P [Eq. (5.6)], the difference between the ratio of the secondary-electron current outside the surface at a given angle θ' to that in the forward direction, and $\cos\theta'$, as function of θ'. The plots are for 2-keV normally incident primary beams and secondary-electron energies E' with respect to the vacuum of (a) $E'=4$ eV, (b) $E'=8$ eV, and (c) $E'=24$ eV. In each figure, curve a shows Stoltz's results, i.e., Eq. (4.14) with $A_0=A_2=T(E,\theta)=1$; curve b shows Stoltz's results when $T(E,\theta)$ is included; curve c shows ψ' [Eq. (4.14)] with the calculated values of A_0 and A_2; curve d shows ψ'' [Eq. (4.27)]; curve e shows ψ''' [Eq. (4.32)].

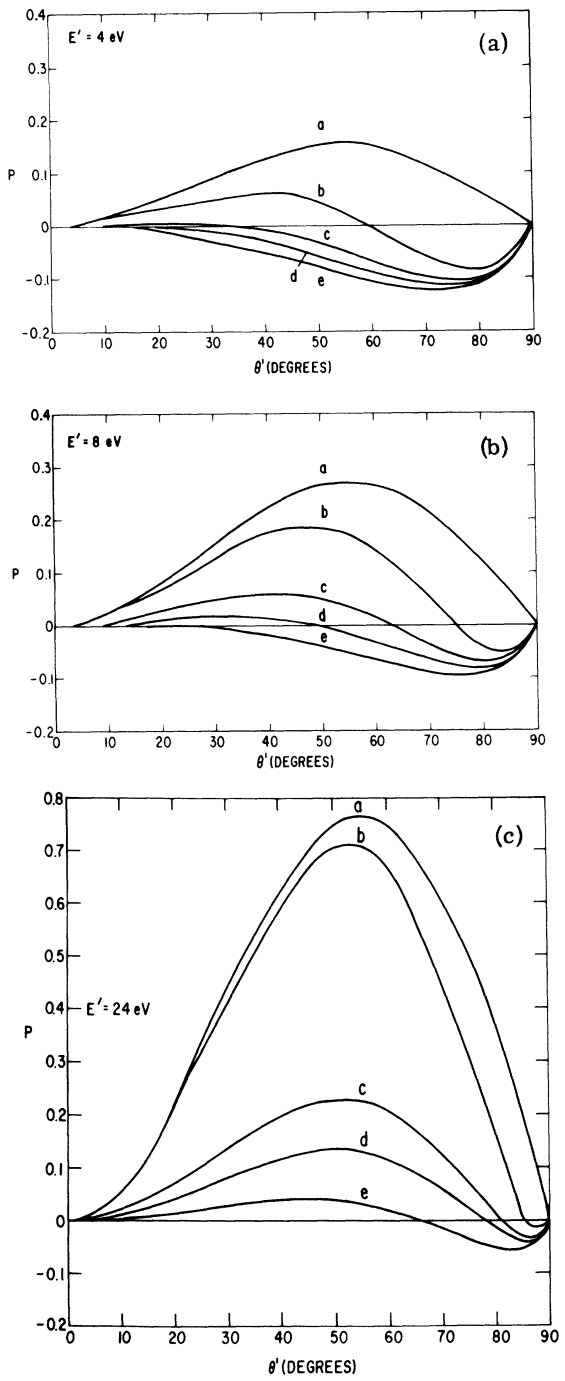

FIG. 14. P [Eq. (5.6)], the difference between the ratio of the secondary-electron current outside the surface at a given angle θ' to that in the forward direction, and $\cos\theta'$, as a function of θ'. The plots are for 10-keV normally incident primary beams and secondary-electron energies E' with respect to the vacuum of (a) $E' = 4$ eV, (b) $E' = 8$ eV, and (c) $E' = 24$ eV. In each figure, curve a shows Stoltz's results, i.e., Eq. (4.14) with $A_0 = A_2 = T(E, \theta) = 1$; curve b shows Stoltz's results when $T(E, \theta)$ is included; curve c shows ψ' with the calculated values of A_0 and A_2; curve d shows ψ'' [Eq. (4.27)]; curve e shows ψ''' [Eq. (4.32)].

versus the external secondary angle θ'. For a cosine law we would have $P = 0$. These results are shown in Figs. 13 and 14 for 2-kev and 10-keV normally incident electrons, respectively. The various figures show ψ', ψ'', and ψ''' together with Stoltz's results (i.e., ψ' with $A_0 = A_2 = 1$) for three secondary energies. Stoltz's results are shown without the transmission factor and with its proper inclusion.

Finally, the results for the pure energy distribution as calculated from ψ', ψ'', and ψ''', as well as results related to those of Stoltz with T included are shown in Figs. 15 and 16 for 2- and 10-keV incident primaries, respectively.

VI. DISCUSSION

Our calculation of the primary-electron distribution differed in several respects from that of Brown which was, however, based on the same equation [Eq. (2.1)]. First, we took the angular variable to be $\cos\theta$, since the angular δ function is well defined in terms of $\cos\theta$. In Brown's work $\delta(\theta)$ appeared which is not well defined since it is multiplied by $\sin\theta$ which vanishes at $\theta = 0$. [Brown took sin(0) as a small positive number in his calculation.] We also used a simpler differencing scheme. Finally, the intervals used were different since we found that we had to use a smaller x interval for stability, and to prevent the spurious spreading of the incoming beam. This was a real restriction on the calculation in terms of computer time.

We have not calculated the x-ray production parameters of major interest to Brown. The comparison (Sec. V) of our results with the total backscattering fraction and energy distribution of backscattered electrons, as calculated by Brown and as measured, indicates, however, that we are somewhat more successful in these predictions. Comparison of our backscattering fractions and F_0 with Monte Carlo calculations indicates that our neglect of large-angle scattering is not of crucial importance for the parameter ranges considered. These scattering events could be included by using Lewis's[11] equation.

Turning now to the production of secondary electrons, the simple free-electron model we have used is hardly original and precludes a discussion of band-structure and crystal-structure effects which would be interesting to pursue in later work. Then, too, the free-electron model underestimates the total yield.

While we feel that the primary-diffusion problem has been treated well, we have not made similar progress with the problem of secondary diffusion. We have obtained two solutions which emphasize either the inhomogeneity of the source function (ψ'') or the presence of the boundary (ψ''').

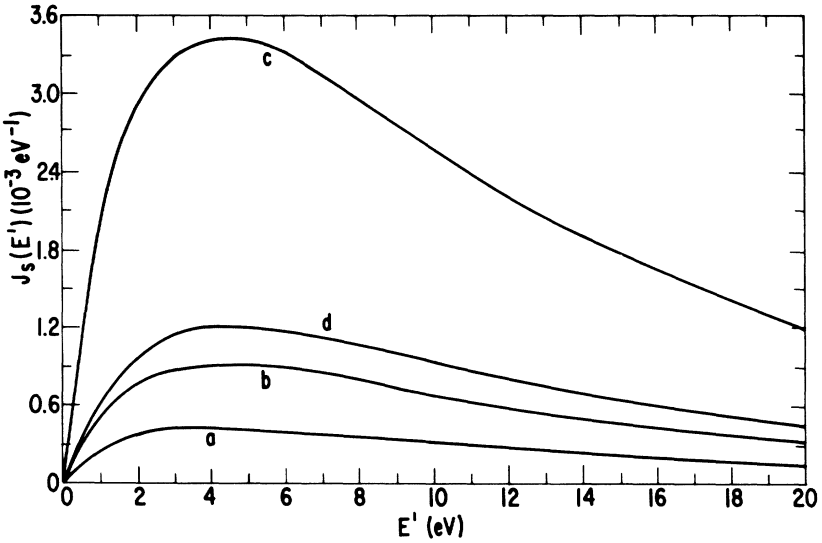

FIG. 15. Pure-energy distribution of secondary electrons normalized to unit primary flux for 2-keV normally incident primaries as a function of secondary-electron energy with respect to the vacuum level. Curve a shows results related to those of Stoltz, i.e., obtained using Eq. (4.14) with $A_0=A_2=1$; curve b shows results obtained from ψ' [Eq. (4.14) with the calculated values of A_0 and A_2]; curve c shows results obtained using ψ'' [Eq. (4.27)]; curve d shows results obtained using ψ''' [Eq. (4.32)].

The latter approximation does, however, include some of the source function spatial inhomogeneity. The difference between the two solutions (Figs. 11 and 12) does resemble an approximate solution to the homogeneous diffusion equation, which is another indication of the accuracy.

VII. CONCLUSIONS

We emphasize that the various approximations used are consistent in predicting several effects of primary-electron diffusion on secondary-electron emission. The primary diffusion increases the yield for all incident beam directions (Figs. 15 and 16). Our calculations all yield significantly smaller deviations from the cosine-law angular distribution than the Stoltz result which neglects primary diffusion. As shown in Figs. 13 and 14, this is particularly pronounced at higher energies. The conclusion is unmistakable that the diffusion of primary electrons is responsible for suppressing any anisotropy in the angular dependence of emitted secondary electrons.

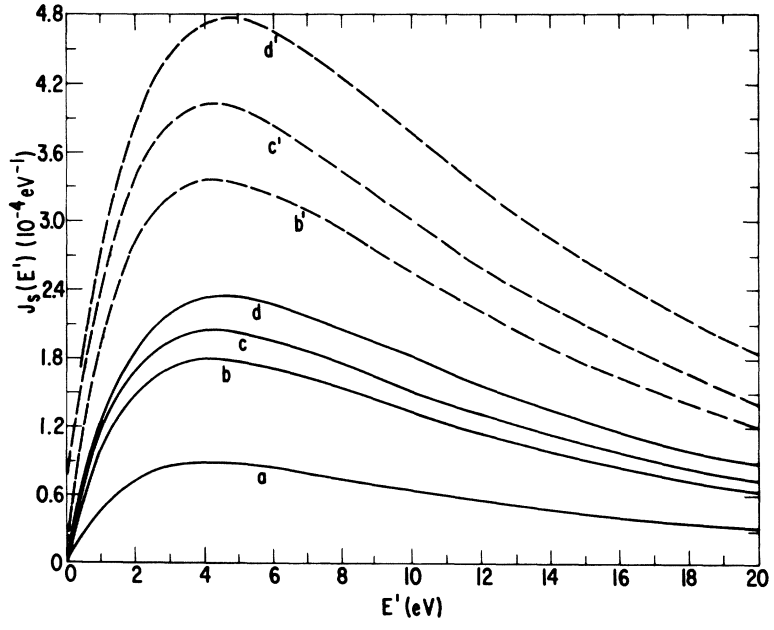

FIG. 16. Pure energy distribution of secondary electrons normalized to unit primary flux for 10-keV normally incident electrons and 10-keV electrons incident at an angle of 53° as a function of secondary-electron energy with respect to the vacuum level. For the normally incident primaries, curve a shows results related to those of Stoltz, i.e., obtained using Eq. (4.14) with $A_0=A_2=1$; curve b shows results obtained using ψ' [Eq. (4.14) with the calculated values of A_0 and A_2]; curve c shows results obtained using ψ'' [Eq. (4.27)]; curve d shows results obtained using ψ''' [Eq. (4.32)]. The corresponding primed curves give the analogous results for the obliquely incident primaries.

[1]O. Hachenberg and W. Brauer, in *Advances in Electronics and Electron Physics XI*, edited by L. Marton (Academic, New York, 1959).
[2]A. J. Dekker, in *Solid State Physics*, edited by F. Seitz and D. Turnbull (Academic, New York, 1959), Vol. 6.
[3]P. R. Thornton, *Scanning Electron Microscopy* (Chapman and Hall, London, 1968).
[4]J. L. H. Jonker, Philips Res. Rept. 6, 372 (1951); 12, 249 (1957).
[5]H. Stoltz, Ann. Physik 3, 197 (1959).
[6]J. Burns, Phys. Rev. 119, 102 (1960).
[7]See, for example, A. I. Titov, Fiz. Tverd. Tela 10, 1891 (1968) [Sov. Phys. Solid State 10, 1489 (1968)]; A. R. Shulman, V. V. Korablev, and Yu. A. Morozov, *ibid.* 10, 1913 (1968) [*ibid.* 10, 1512 (1968)]; A. B. Laponsky and N. R. Whetten, Phys. Rev. 120, 801 (1960).
[8]See, for example, A. J. Dekker, Phys. Rev. Letters 4, 55 (1960); R. M. Stern and H. Taub, *ibid.* 20, 1340 (1968); H. Taub, R. M. Stern, and V. F. Dvoryankin, Phys. Status Solidi 33, 573 (1969).
[9]H. A. Bethe, M. E. Rose, and L. P. Smith, Proc. Am. Phil. Soc. 78, 573 (1938).
[10]H. S. Snyder and W. T. Scott, Phys. Rev. 76, 220 (1949).
[11]H. W. Lewis, Phys. Rev. 78, 526 (1950).
[12]L. V. Spencer, Phys. Rev. 98, 1597 (1955).
[13]G. D. Archard, J. Appl. Phys. 32, 1505 (1961).
[14]T. E. Everhart, J. Appl. Phys. 31, 1483 (1960).
[15]R. F. Dashen, Phys. Rev. 134, A1025 (1964).
[16]M. Green, Proc. Phys. Soc. (London) 82, 204 (1963).
[17]D. B. Brown, DSc. thesis (MIT, 1965) (unpublished); *Quantitative Electron Probe Microanalysis*, Natl. Bur. Std. Spec. Publ. 298, 63 (1968); D. B. Brown and R. E. Ogilvie, J. Appl. Phys. 37, 4429 (1966).
[18]H. W. Streitwolf, Ann. Physik 3, 183 (1959).
[19]P. A. Wolff, Phys. Rev. 95, 56 (1954).
[20]J. Weymouth, Phys. Rev. 84, 766 (1951).
[21]D. B. Brown and R. E. Ogilvie, J. Appl. Phys. 35, 309 (1964).
[22]N. F. Mott and H. S. W. Massey, *The Theory of Atomic Collisions* (Oxford U. P., New York, 1949).
[23]R. D. Richtmyer and K. W. Morton, *Difference Methods for Initial Value Problems* (Interscience, New York, 1962).
[24]Higher-order corrections have been considered by G. I. Amelio and E. J. Scheibner, in *The Structure and Chemistry of Solid Surfaces*, edited by G. A. Somorjai (Wiley, New York, 1969),
[25]E. Jahnke and F. Emde, *Tables of Functions* (Dover, New York, 1945).
[26]See, for example, P. H. Cutler and J. C. Davis, Surface Sci. 1, 194 (1964).
[27]E. F. H. StG. Darlington, in *Fifth International Congress on X-Ray Optics and Microanalysis, Tubingen*, 1968, edited by G. Mollenstedt and K. H. Gaukler (Springer-Verlag, New York, 1969), p. 76.
[28]H. E. Biship, *X-Ray Optics and Microanalysis* (Hermann, Paris, 1966), p. 153.
[29]H. E. Bishop, Proc. Phys. Soc. (London) 85, 855 (1965).
[30]See, e.g., J. J. Quinn, Phys. Rev. 126, 1453 (1962).

PHYSICAL REVIEW B VOLUME 5, NUMBER 11 1 JUNE 1972

Analysis of the Fe^{3+}-V_O Center in the Tetragonal Phase of $SrTiO_3$

Th. von Waldkirch, K. A. Müller, and W. Berlinger
IBM Zurich Research Laboratory, 8803 *Rüschlikon, Switzerland*
(Received 3 January 1972)

The paramagnetic resonance spectrum of the iron oxygen-vacancy (Fe^{3+}-V_o) pair in the tetragonal $I4/mcm$ phase of $SrTiO_3$ at 78 °K is analyzed in detail. The spectra observed at K band are fully accounted for using the accepted structural properties of the crystal in the low-temperature phase. Whereas in the high-temperature cubic O_h^1 phase the Fe^{3+}-V_O spectra are axial, in the $D_{4h}^{18}-I4/mcm$ phase second-order perturbation terms of an orthorhombic $E(T)(S_x^2-S_y^2)$ term have to be taken into account with $E(T)=1.82\varphi^2(T)$ cm^{-1}, $\varphi(T)$ being the intrinsic rotational (order) parameter of the transition measured in radians. The analytically well understood spectrum justifies its use for the analysis of the structural phase transition observed in $SrTiO_3$ under applied stress and for the investigation of critical phenomena.

I. INTRODUCTION

In this paper a detailed analysis of the paramagnetic resonance spectrum of the Fe^{3+}-V_O center—a charge-compensated Fe^{3+} impurity—in strontium titanate at 78 °K is presented. The resonance of this center has been attributed to a three-valent-iron impurity substitutional for a Ti^{4+} ion with a nearest-neighbor oxygen vacancy, and analyzed previously in the cubic phase by Kirkpatrick, Müller, and Rubins,[1] hereafter referred to as KMR. The analysis consisted essentially of the Fe^{3+}-ground-state splitting in the presence of a large axial crystal-field term $D[S_z^2-\frac{1}{3}S(S+1)]$ with the z axis parallel to one of the three equivalent $\langle 100\rangle$ crystal axes. It has subsequently been refined by two groups by taking into account fourth-order terms in the spin Hamiltonian yielding agreement with the essential point of the KMR investigation.[2,3] Since then the center was also observed in $BaTiO_3$[4] and $KTaO_3$,[5] and the same kind of centers have now also been observed for other transition-metal ions such